Studying Plasmon Dispersion of MXene for Enhanced Electromagnetic Absorption

Xiangdong Guo, Ning Li, Chenchen Wu, Xiaokang Dai, Ruishi Qi, Tianyu Qiao, Tuoyi Su, Dandan Lei, Nishuang Liu, Jinlong Du, Enge Wang, Xiaoxia Yang, Peng Gao,* and Qing Dai**

2D metal carbides and nitrides (MXene) are promising candidates for electromagnetic (EM) shielding, saturable absorption, thermal therapy, and photocatalysis owing to their excellent EM absorption. The plasmon resonances in metallic MXene micro/nanostructures may play an important role in enhancing the EM absorption; however, their contribution has not been determined due to the lack of a precise understanding of its plasmon behavior. Here, the use of high-spatial-resolution electron energy-loss spectroscopy to measure the plasmon dispersion of MXene films with different thicknesses is reported, enabling accurate analysis of the EM absorption of complex MXene structures in a wide frequency range via a theoretical model. The EM absorption of MXene can be excited at the desired frequency by controlling the momentum (e.g., the sizes of the nanoflakes for EM excitation) as the strength can be enhanced by increasing the layer number and the interlayer distance in MXene. For example, a 3 nm interlayer distance can nearly double the plasmon-enhanced EM absorption in MXene nanostructures. These findings can guide the design of advanced ultrathin EM absorption materials for a broad range of applications.

1. Introduction

Ultrathin and flexible electromagnetic (EM) shielding materials are widely required for eliminating EM interference in electronic devices[1] such as handheld radios and computers, medical imaging equipment, broadband routers, wearable consumer electronics, and automotive sensing equipment.[1c,d,2] For these devices, the EM interference diminishes electrical performance, introduces noise signals, slows data exchange rates, and can even interrupt the function of devices. Recently, 2D transition metal carbides and nitrides (MXene) have demonstrated exceptional shielding ability,[1a,b,e,3] due to their high EM absorption, lightweight, high strength, and ease of manufacture.[2,4]

$Ti_3C_2T_x$ is a typical MXene material, and T_x represents the surface terminated parts, such as —O, —OH, or —F.[2a,5] Its intrinsic metallic nature[6] combined with abundant surface termination and a laminate architecture contributes to achieving a high EM shielding performance.[1a,7] In each layer, the incident EM waves are partially reflected due to the high intrinsic electrical conductivity of MXene, and the remaining waves are then partially dissipated due to the interaction of the EM-dirven electrons with the MXene lattice defects.[8] This process can be repeated in the laminate architecture of MXene until the penetrated EM waves are competely absorbed.[9] This EM shielding performance can be further improved by introducing porous structures with partial oxidation in annealed MXene, but the observed increase cannot be fully explained within the framework of existing shielding theories.[1b] These phenomena imply that there must be other dissipation channels in addition to classical reflection and absorption of EM waves.

One possible explanation is the plasmon-induced EM absorption, which has been observed in MXene[10] as well as metals[11]

X. Guo, C. Wu, X. Dai, X. Yang, Q. Dai
CAS Key Laboratory of Nanophotonic Materials and Devices
CAS Key Laboratory of Standardization and Measurement for Nanotechnology
CAS Center for Excellence in Nanoscience
National Center for Nanoscience and Technology
Beijing 100190, China
E-mail: yangxx@nanoctr.cn; daiq@nanoctr.cn

X. Guo, C. Wu, X. Dai, X. Yang, Q. Dai
Center of Materials Science and Optoelectronics Engineering
University of Chinese Academy of Sciences
Beijing 100049, China

The ORCID identification number(s) for the author(s) of this article can be found under https://doi.org/10.1002/adma.202201120.

N. Li, R. Qi, T. Qiao, J. Du, P. Gao
Electron Microscopy Laboratory
School of Physics
Peking University
Beijing 100871, China
E-mail: p-gao@pku.edu.cn

T. Su, D. Lei, N. Liu
School of Physics
Wuhan National Laboratory for Optoelectronics (WNLO)
Huazhong University of Science and Technology (HUST)
Wuhan 430074, P. R. China

E. Wang, P. Gao
International Center for Quantum Materials
Interdisciplinary Institute of Light-Element Quantum Materials and Research Center for Light-Element Advanced Materials
Collaborative Innovation Center of Quantum Matter
Beijing 100871, China

and other 2D materials.[12] Plasmons can be effectively excited in the annealed Ti_3CNT_x MXene with a porous structure and partial oxidation, which can provide the required momentum compensation,[1b] and these resonances in a wide frequency range should play an important role in determining the EM absorption. However, the characterization of the plasmon dispersion (i.e., the frequency (ω)–momentum (q) relationship, which is an intrinsic characteristic of plasmons) in few-layer MXene remains challenging, because the plasmons are too lossy to be precisely observed by either near-field optical microscopy or far-field optical spectroscopy.[13]

Here, we use electron energy-loss spectroscopy integrated in a scanning transmission electron microscope (STEM-EELS) to characterize the plasmon dispersion of MXene nanoflakes. By comparing the different dispersions, the MXene layer number and momentum are found to have an important impact on the plasmon-induced EM absorption. Numerical simulations demonstrate that the plasmon-enhanced EM absorption can be increased by increasing the layer number and the interlayer distance for a given momentum. A 300-layer MXene nanostructure with a 3 nm interlayer distance is theoretically demonstrated to reach an EM absorption of nearly 100%. Our work demonstrates the large plasmon-induced EM absorption of MXene in a broad band, thus providing a guidance for developing advanced EM absorption materials and designing ultrathin EM devices, such as EM absorbers, EM shielding devices, and photothermal devices.

2. Dispersion of Ultra-Broadband Plasmons in Few-Layer MXene Film

The momentum compensation is required to excite plasmons; it can be achieved by optically coupling structures or moving electrons. Monochromatic STEM–EELS is employed to detect the broadband surface plasmons in MXene by providing a large momentum compensation from the fast electrons. The schematic diagram of the experimental setup is shown in **Figure 1**a. The spatial resolution is less than 1 nm, and the energy resolution is less than 10 meV at a voltage of 30 kV. Few-layer $Ti_3C_2T_x$ MXene, with carbon atoms packed in a hexagonal structure with Ti layers and passivated with −O, −OH, and −F terminations (see Figure), is prepared through exfoliation method in liquid phase from synthesized $Ti_3C_2T_x$ MXene flakes and transferred on the transmission electron microscopy (TEM) grids (details are provided in the Experimental Section). The high-angle annular dark-field (HAADF) image of the synthesized MXene flake in Figure 1c demonstrates the high quality of the prepared MXene. According to the elemental composition analysis (details are provided in Figure S1, Supporting Information), the ratio of oxygen atoms to fluorine atoms in terminated surface moieties (T_x) is around 6:1. The few-layer MXene films are suspended on the TEM grids to avoid the influence of dielectric substrate and obtain the intrinsic MXene plasmon signal.

A set of typical EELS spectra are measured in Figure 1d with the electron beam moving from vacuum to interior of the MXene film with a step length of ≈6 nm. The corresponding thickness (t) of MXene is ≈4.5 nm (details are provided in Figure S2, Supporting Information), which approximately corresponds to three layers of MXene as each layer is ≈1.3 nm. Two resonance peaks can be observed in the EELS spectra in Figure 1d, which are identified as modes I and II. Interestingly, there is only one single resonance peak (mode I) on the EELS spectra when the electron beam passes through the vacuum. The resonance frequency of mode I remains nearly constant even when the electron beam moves. By contrast, the peak corresponding to mode II only appears when the electron beam is incident on the interior of the MXene film, and its frequency undergoes a redshift when the electron beam moves away from the MXene/vacuum edge. Furthermore, numerical simulations based on the finite element method (FEM) are performed to study the characteristics of MXene plasmons from a fundamental perspective. The optical parameters utilized for the MXene film (see Figure S3, Supporting Information) and the EELS simulation model are presented in Supplementary Notes S1 and S2 (Supporting Information), in which the dielectric function is derived from the macroscopic average properties of the material. The difference between the two plasmon modes in the EELS spectra is shown in Figure 1e. The mode II peak is a plasmon signal that travels to the edge and is then reflected by the edge to interfer with the excited plasmon, while the mode I peak is a noninterference plasmon signal that travels along the other directions.[14] The mode II peak undergoes a gradual redshift and approaches mode I peak; eventually, the two modes merge into one peak.

To deeply analyze these two plasmon modes, the waveguide model of FEM simulation is utilized to calculate the EM field distribution (i.e., E_z and H_x).[15] As shown in Figure S5, the EM field is highly confined on the surface (≈100 nm) of MXene which is a typical feature of surface plasmon evanescent field. The only one zero-point in the H_x profile implies that both modes I and II are the fundamental surface transverse magnetic (SM_0) mode.[14] These highly confined plasmon modes as well as the large imaginary part of MXene dielectric function anticipate ultrastrong EM absorption in MXene. It is demonstrated by the fast damping of the propagating plasmon that is absorbed within one wavelength (details are provided in Figure S5b,c and Note S2 in the Supporting Information).

To further analyze the characteristics of MXene plasmon at different frequencies (ω), the collected EELS spectra (step length is ≈1.5 nm) are mapped in momentum space (q) and plotted in Figure 1f. Then, an instructive way to visualize the dispersion (ω–q) is via a false-color plot of $\mathrm{Im}(r_p)$.[16] The $\mathrm{Im}(r_p)$ of MXene is obtained according to the theory of multilayer film interference (Supplementary Note S3 (Supporting Information), and the maximum values of $\mathrm{Im}(r_p)$ at different frequencies are extracted and plotted in Figure 1f (blue curve). It can be seen that these values are in good agreement with the experimental results. Therefore, the ultra-broadband plasmon responses in the frequency domain below the near-infrared range and especially in the telecommunication band of MXene are demonstrated. Most importantly, it is the first time that the dispersion of MXene plasmon, the frequency range of plasmon resonances, and the corresponding wavelength compression are experimentally demonstrated.

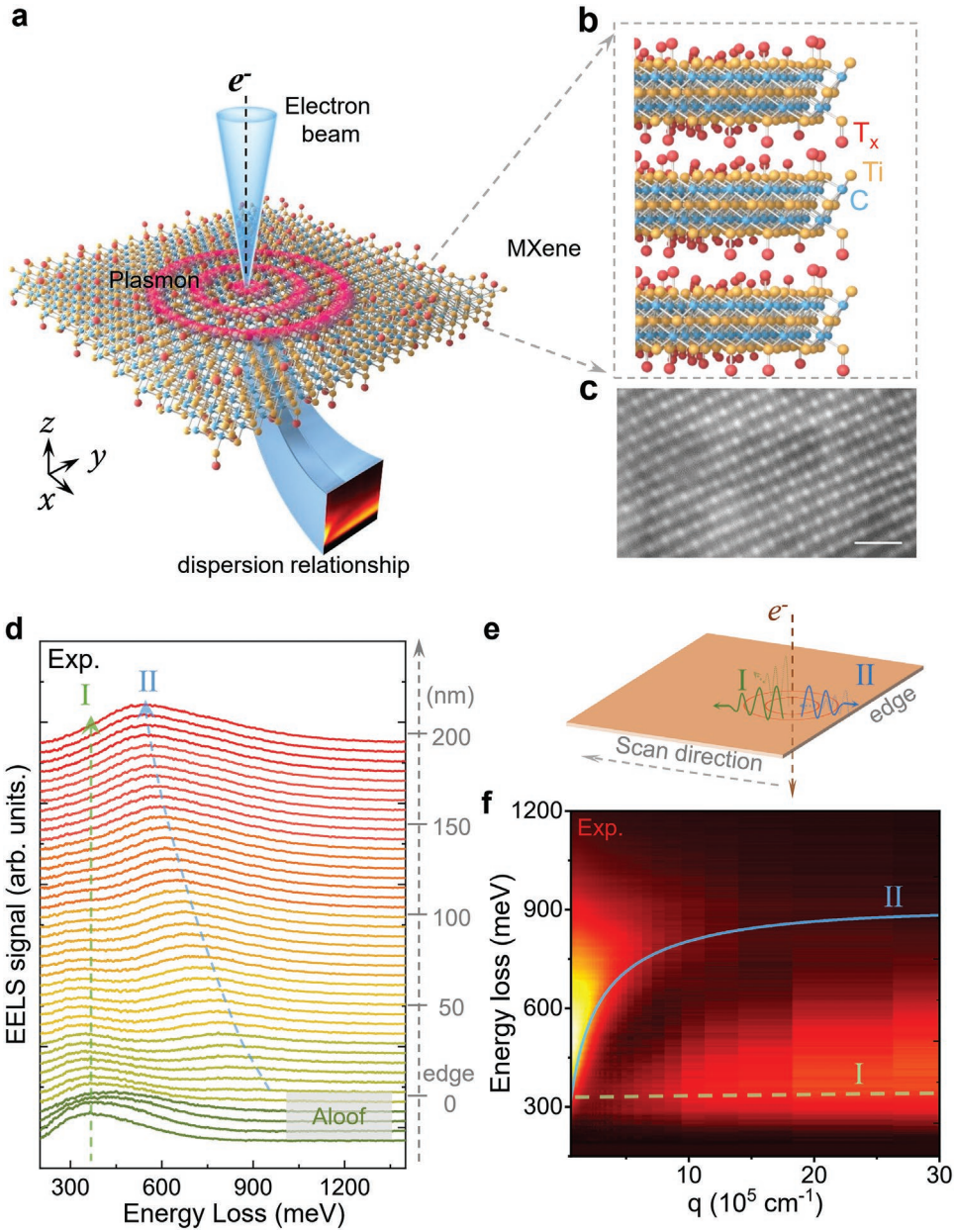

Figure 1. a) Schematic diagram of electron-excited MXene plasmon via STEM–EELS. b) Magnified view of the diagram of the lattice structure and the chemical compositions of MXene. c) HAADF image of MXene film. The scale bar is 0.5 nm. d) Experimental EELS spectra for the different spatial positions of the electron beam, from the vacuum (Aloof) to the bulk of MXene. e) Schematic illustration of plasmons (mode I and II) are obtained when the electron beam moves from vacuum to the interior of MXene film. f) Dispersion of MXene plasmons. The color image is obtained by transforming the experimental EELS spectra of MXene into the momentum space, and the solid line represents the dispersion calculated based on the theoretical model. The frequency can cover the range below the near-infrared region, which includes the telecommunication frequency (telecom. freq.). The thickness of MXene is ≈4.5 nm.

3. Plasmon-Enhanced EM Absorption of MXene with Varied Thicknesses

The stacked structure has been demonstrated to be a key factor for the ultrastrong EM absorption of MXene.[17] We take a folded monolayer MXene film with a monolayer/folded two-layer interface (**Figure 2**a) as an example. The folded bilayer region of MXene has a thickness of ≈2.6 nm and a width of ≈145 nm, and the monolayer region has a thickness of ≈1.3 nm (details are provided in Figure S2c,d, Supporting Information). A series of EELS spectra are measured as the electron beam moves from the vacuum to the folded region and then the monolayer region, as shown in Figure 2a. The EELS spectra measured at the edge (bilayer MXene/the air) and the boundary (bilayer MXene/monolayer MXene) are shown as red curves highlighted. The mode II redshifts when the electron beam moves to inside of the folded MXene, but the rates of redshift at various regions are different obviously. An anticrossing

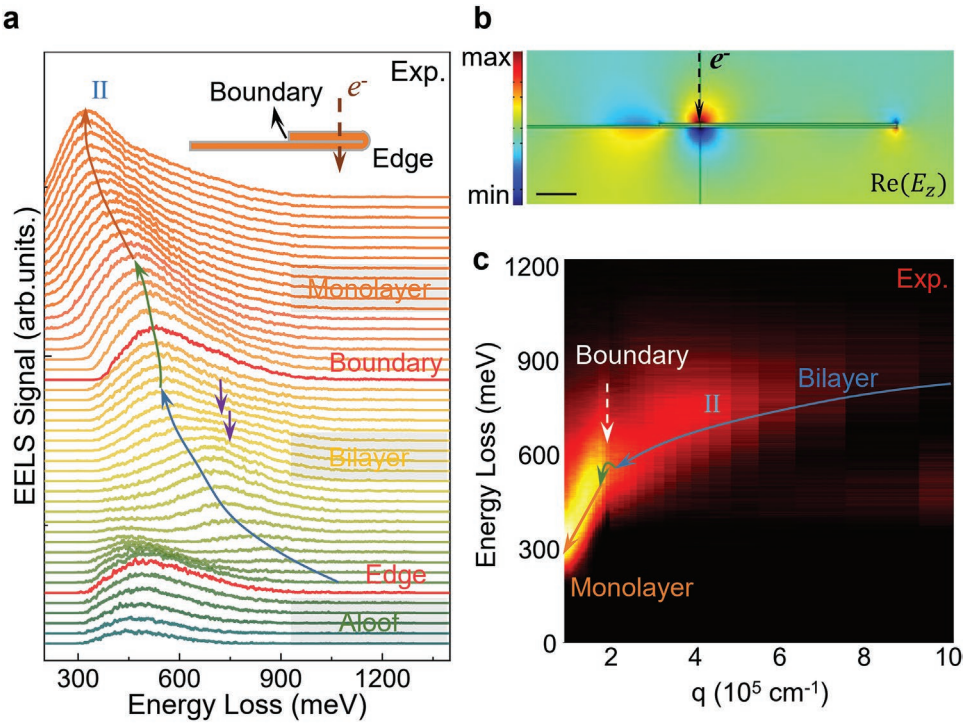

Figure 2. a) Experimental EELS spectra in folded monolayer MXene. The two EELS spectra measured at the edge (bilayer MXene/air) and boundary (bilayer MXene/monolayer MXene) are highlighted in red. The blue, green, and orange solid arrows are guides for indicating the shift of peaks. The purple arrows indicate the small bulge features in the EELS spectra. b) Extracted electric field distribution (Re(E_z)) of folded monolayer MXene plasmon in the *x*–*z*-plane at ≈460 meV. The scale bar is 25 nm. c) Plasmon dispersion of the folded monolayer MXene. The experimental EELS spectra are collected and plotted in momentum space. The solid lines are a guide to the eye for plasmon dispersion.

phenomenon appears in EELS spectra at the interface between monolayer and bilayer MXene that is similar to the condition of plasmon–phonon coupling. Moreover, it should be also emphasized that there are some interesting features in the EELS spectra of the folded bilayer MXene: asymmetrical spectral line profile and small bulge (indicated by the purple arrow in Figure 2a), which mainly originate from the interference effect of a plasmon induced by the monolayer/bilayer boundary.[14] The plasmon interference with the boundary-reflected plasmon can be further demonstrate by the fact that the monolayer/bilayer boundary and bilayer MXene/air edge have strong interferometric resonance-generated EM field distribution (Re(E_z)) and EM energy (|E|), as shown in Figure 2b (details are provided in Figure S6, Supporting Information).

The dispersion of folded monolayer MXene is also obtained by converting the EELS data from the spectrum to momentum space,[18] where the boundary interference phenomenon is clearly revealed, as highlighted by the white dashed arrow in Figure 2c. It is obviously different from the smooth dispersion curve of a pure bilayer MXene film (Figures S7 and S8, Supporting Information). Furthermore, the full width at half maximum (FWHM) of the EELS spectra in bilayer MXene are much larger than those in monolayer MXene in Figure 2c, which hints the larger plasmon-enhanced EM absorption of a thicker MXene since the FWHM is proportional to the damping of plasmon and thus the EM absorption.[19]

The measured EELS spectra of MXene films with different thicknesses (1.3 nm, 2.8 nm, 4.5 nm, 5.1 nm, 6.2 nm, and 7.8 nm) are prepared to quantitively analyze the thickness effects on the EM absorption. The number of layers can be inferred from the measured thickness of MXene. The thickness of monolayer MXene in our experiment is ≈1.3 nm. Therefore, the thickness of 2.8 nm is a bilayer, the thickness of 4.5 nm and 5.1 nm are trilayers, the thickness of 6.2 nm is a four-layer, and the thickness of 7.8 nm is a five-layer. The FWHMs of MXene plasmon with different thicknesses are extracted from the EELS spectra via Lorenz function fitting (details are provided in Figure S13 in the Supporting Information), which directly reflect the change of plasmon-enhanced EM absorption as a function of MXene thickness in **Figure 3**a. In particular, the plasmon-enhanced EM absorption increases as the thickness increases, but the absorption efficiency of each layer in multilayer MXene continuously decreases upon increasing the thickness (Figure S16g, Supporting Information). To further analyze the thickness-determined plasmon-enhanced EM absorption in MXene, the dispersions of MXene with different thicknesses are compared. In Figure 3b, the EM field confinement of plasmon decreases as the thickness increases, which induces the decreasing EM absorption of each layer. In addition, we predict that the plasmon dispersion and confinement remain the same as the film thickness increases to about 390 nm (i.e. 300-layer). This phenomenon limits considerably the possibility to further enhancing absorption of plasmon. To overcome the challenge, improving plasmon confinement is important. Thus, increasing the interlayer distance of MXene can weaken interlayer coupling and thus enable a stronger field confinement

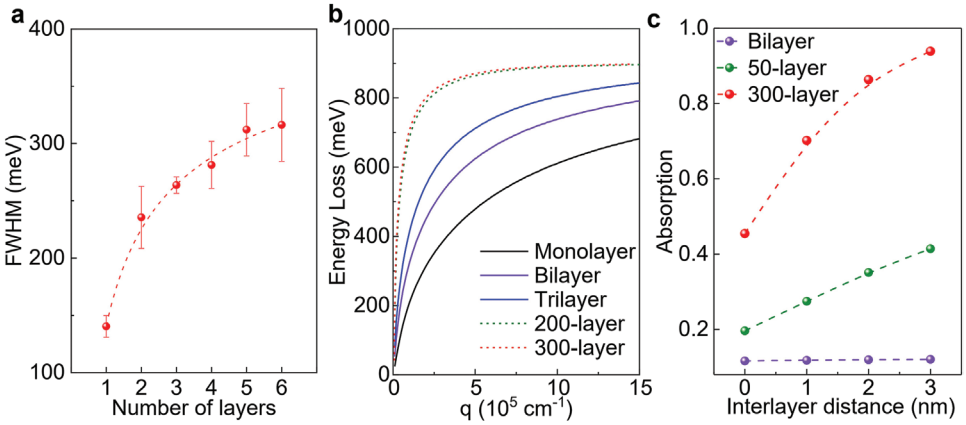

Figure 3. a) FWHM of plasmons (red balls) as a function of the number of MXene. b) Plasmon dispersion of MXene with different numbers of layers (details are provided in Figures S7–S12, Supporting Information). c) Maximum intensity of plasmon-enhanced EM absorption as a function of the interlayer distance.

(Figure S9, Supporting Information). This provided an efficient method to optimize the plasmon-enhanced EM absorption.

4. The Interlayer Distance Design for an Ultrathin EM Absorber with MXene Plasmon

In practical applications of EM absorbers such as EM shielding devices and photothermal photocatalysis devices, the stacked structures of MXene flakes are often used to exploit the absorption cumulation phenomenon. It is necessary to study the effects of stacking (e.g., the interlayer distance and layer number) due to the plasmon coupling in different structures, which has been demonstrated to largely enhance the EM shielding.[1b] We first calculate the dispersion of bilayer MXene with the interlayer distance varying from 0 to 10 nm (Figure S9, Supporting Information). The dispersions of bilayer MXene are gradually approaching the dispersion of individual monolayer MXene as the interlayer distance increases, which results in higher field confinement of the EM waves and so the stronger absorption. This effect is more pronounced for thicker samples since the confinement of the plasmon EM field is reduced more severely. To illustrate this aspect, the plasmon-enhanced absorption spectra in periodic MXene nanostrips with different interlayer distances and thicknesses (details are provided in Figures S15 and S16, Supporting Information) are simulated. Figure 3c shows the plasmon-enhanced EM absorption as a function of the interlayer distance in three representative MXene samples. As seen, an interlayer distance of 3 nm can nearly double the EM absorption intensity, and a 300-layer MXene nanoribbon can achieve nearly perfect absorption. Combined with the evolution of dispersion as the function of interlayer distance, this result shows that plasmon-enhanced EM absorption in MXene flakes increases monotonically as the interlayer distance increases. Besides, it is not necessary to accurately control the interlayer distance for practical applications.

Finally, we compare the plasmon in EELS measurement and in practical applications of EM absorbers, such as EM shielding devices, photothermal devices, and photocatalysis devices. The only difference between the EELS-measured plasmons and the EM-excited plasmons is the manner in which the plasmons are excited, while the plasmon dispersion and loss are determined by the material. In EELS experiments, the plasmons are excited by the incident electron beam, and the momentum of the resonant plasmon can be modulated by the distance of the incident electron beam to the edge of the MXene flake ($q = \pi/x$, x is the distance from the electron beam position to the material edge).[18] For practical applications, localized plasmon resonance can be directly excited in MXene flakes by EM waves, and the plasmon momentum can be modulated by the size (W) of flakes via $q = \pi/W$.[20] Given the plasmon dispersion of MXene as measured by EELS and corroborated by the theoretical calculation, we can design the size of the MXene flakes to achieve plasmons with target frequency. MXene nanostructures with arbitrary sizes may be obtained via controlled chemical exfoliation and etching of grown MXene films as well as traditional micro-/nanofabrication techniques, such as focused ion beam, electron beam lithography, and reactive ion etching in grown MXene films.[2a,4b,6a,13d] Moreover, we theoretically studied the effects of interlayer distance due to the limitation of existing experimental methods since the stacked structures of MXene flakes are often used. The calculation gives a very general rule for how to design the MXene structures, i.e., the plasmon absorption intensity increases monotonically with the number of layers, and it increases with increasing interlayer distance with progressively slower rates. The interlayer distance can be modulated by chemical etching to intercalate cationic surfactant,[21] mixing MXene flakes with other dielectric flakes such as hexagonal boron nitride flakes,[22] and thermal annealing.[1b,4b]

5. Conclusion

We have experimentally measured the broadband plasmon-enhanced EM absorption (below 900 meV) and the plasmon dispersions in individual MXene flakes with varied thicknesses via STEM-EELS. The measured plasmon dispersions enable our theoretical model to accurately analyze the EM absorbtion of

complex MXene structures with different thicknesses, interlayer distances, and momentum values over a wide frequency range. The obtained result is useful as a guide for the MXene structure design (e.g., the size of the MXene micro/nanostructures) for exciting plasmons at the desired frequency. Moreover, the EM absorption can be improved either by increasing the number of MXene layers or increasing the interlayer distance. For example, as the interlayer distance increases from 0 to 3 nm, the calculated plasmon-enhanced absorption increases by more than a factor of two, and a nearly perfect EM absorption is achieved in a 300-layer MXene nanostructure. These ultrathin and flexible MXene materials with broadband plasmon-enhanced absorption properties provide a promising platform for realizing high-performance photonics and optoelectronic devices.

6. Experimental Section

MXene Preparation for the TEM Experiments: Suspensions of MXene ($Ti_3C_2T_x$) were prepared using conventional chemical synthesis methods.[23] The suspended MXene could be prepared by using droplets to transfer onto the 3 mm lacy carbon TEM grid. Finally, before the STEM experiment, the sample was annealed in a vacuum chamber at 160 °C for 8 h to remove possible hydroxide contamination.

EELS and Imaging Experiments: The EELS experiments were acquired using a Nion U-HERMES200 electron microscope with a monochromator that operated at 30 kV to avoid any damage to MXene materials.[24] A convergence semiangle α = 20 mrad and a collection semiangle β = 25 mrad were employed for all datasets. In this setting, the spatial resolution was ≈2 nm, with an energy resolution up to 5 meV. However, a relatively large energy dispersion of 1 meV per channel was used to include all plasmon signals, thus the actual energy resolution was limited to ≈7.5 meV. The acquisition times were chosen as 600 ms per pixel to improve the signal-to-noise ratio of the spectra, making the zero-loss peak (ZLP) slightly saturated. The HAADF images were acquired using Nion U-HERMES200 operated at 60 kV.[14,25]

EELS Data Processing: All the acquired vibrational spectra were processed by using a custom-written MATLAB code and Gatan Microscopy Suite. More specifically, the EEL spectra were first aligned by their normalized cross-correlation. Subsequently, the block-matching and 3D filtering (BM3D) algorithms were adopted to remove the Gaussian noise. The background arising from both the tail of the ZLP and the noncharacteristic phonon losses was fitted with a modified Peason-VII function with two fitting windows and then subtracted in order to obtain the vibrational signal. The spectra were summed along the direction parallel to the interface for obtaining line-scan data with a good signal-to-noise ratio.[14,25]

Theoretical Calculations: We employ a finite element method implemented in COMSOL Multiphysics to simulate the EELS spectra. The Radio Frequency Toolbox is used for performing retarded simulations (solving Maxwell's equations) to evaluate the electric field in the presence of a MXene. The dielectric functions of the MXene are average values obtained from large-area films, which could approximately calculate the plasmon response (details are provided in Figure S3 and Supporting Note S1, Supporting Information).[6a]

By following a well-established procedure, a current source is used to represent the electron beam along the direction perpendicular to the sample.[26] When electron beam stricks on the sample, an induced field $\mathbf{E}^{\text{ind}}(\mathbf{r},t) = \mathbf{E}(\mathbf{r},t) - \mathbf{E}_0(\mathbf{r},t)$ is generated, where $\mathbf{E}(\mathbf{r},t)$ is the total field distribution, as determined by the optical response of the MXene. Finally, we calculate the loss probability (by using Edge Probe, Integral applied along the electron trajectory) according to:[27]

$$\Gamma_{\text{EELS}}(\omega) = \frac{e}{\pi\hbar\omega}\int \text{Re}\left\{\exp\left(-\frac{i\omega z}{v}\right)E_z^{\text{ind}}(z,\omega)\right\}\text{d}z \quad (1)$$

Therefore, the EELS spectra are simulated according to the equation describing electrons passing the MXene and the corresponding results are presented in Figure S4 and Note S2, Supporting Information.

Supporting Information

Supporting Information is available from the Wiley Online Library or from the author.

Acknowledgements

X.G., N.L., and C.W. contributed equally to this work. This work was supported by the National Key R&D Program of China (Grant Nos. 2021YFA1201500, 2021YFA1400500), the National Natural Science Foundation of China (Grant Nos. 51925203, 52022025, 52102160, 51972074, 52125307, 11974023, 52021006, T2188101, and U2032206), the Strategic Priority Research Program of the Chinese Academy of Sciences (Grant Nos. XDB30000000 and XDB36000000), the Youth Innovation Promotion Association C.A.S., C.A.S. Interdisciplinary Innovation Team (Grant No. JCTD-2018-03), the "2011 Program" from the Peking–Tsinghua–IOP Collaborative Innovation Center of Quantum Matter, and the Open Project of Nanjing University (Grant No. M34034). The authors also acknowledge the Electron Microscopy Laboratory of Peking University for the use of electron microscopes.

Conflict of Interest

The authors declare no conflict of interest.

Data Availability Statement

The data that support the findings of this study are available from the corresponding author upon reasonable request.

Keywords

electromagnetic absorption, MXene, nanoflakes, plasmon dispersions

[1] a) F. Shahzad, M. Alhabeb, C. B. Hatter, B. Anasori, S. M. Hong, C. M. Koo, Y. Gogotsi, *Science* **2016**, *353*, 1137; b) A. Iqbal, F. Shahzad, K. Hantanasirisakul, M.-K. Kim, J. Kwon, J. Hong, H. Kim, D. Kim, Y. Gogotsi, C. M. Koo, *Science* **2020**, *369*, 446; c) Z. Chen, C. Xu, C. Ma, W. Ren, H. M. Cheng, *Adv. Mater.* **2013**, *25*, 1296; d) N. Yousefi, X. Sun, X. Lin, X. Shen, J. Jia, B. Zhang, B. Tang, M. Chan, J. K. Kim, *Adv. Mater.* **2014**, *26*, 5480; e) T. Yun, H. Kim, A. Iqbal, Y. S. Cho, G. S. Lee, M. K. Kim, S. J. Kim, D. Kim, Y. Gogotsi, S. O. Kim, C. M. Koo, *Adv. Mater.* **2020**, *32*, 1906769.

[2] a) A. VahidMohammadi, J. Rosen, Y. Gogotsi, *Science* **2021**, *372*, eabf1581; b) B. Anasori, M. R. Lukatskaya, Y. Gogotsi, *Nat. Rev. Mater.* **2017**, *2*, 16098.

[3] J. Liu, Z. Liu, H. B. Zhang, W. Chen, Z. Zhao, Q. W. Wang, Z. Z. Yu, *Adv. Electron. Mater.* **2020**, *6*, 1901094.

[4] a) M. Naguib, M. W. Barsoum, Y. Gogotsi, *Adv. Mater.* **2021**, *33*, e2103393; b) J. Jeon, Y. Yang, H. Choi, J.-H. Park, B. H. Lee, S. Lee, *Nanophotonics* **2020**, *9*, 1831.
[5] V. Kamysbayev, A. S. Filatov, H. Hu, X. Rui, F. Lagunas, D. Wang, R. F. Klie, D. V. Talapin, *Science* **2020**, *369*, 979.
[6] a) K. Chaudhuri, M. Alhabeb, Z. Wang, V. M. Shalaev, Y. Gogotsi, A. Boltasseva, *ACS Photonics* **2018**, *5*, 1115; b) H. Lashgari, M. R. Abolhassani, A. Boochani, S. M. Elahi, J. Khodadadi, *Solid State Commun.* **2014**, *195*, 61.
[7] a) Y. Zhu, J. Liu, T. Guo, J. J. Wang, X. Tang, V. Nicolosi, *ACS Nano* **2021**, *15*, 1465; b) L. Liang, Q. Li, X. Yan, Y. Feng, Y. Wang, H. B. Zhang, X. Zhou, C. Liu, C. Shen, X. Xie, *ACS Nano* **2021**, *15*, 6622.
[8] Q. Song, F. Ye, L. Kong, Q. Shen, L. Han, L. Feng, G. Yu, Y. Pan, H. Li, *Adv. Funct. Mater.* **2020**, *30*, 2000475.
[9] H. Ren, S. Wang, X. Zhang, Y. Liu, L. Kong, C. Li, X. Lu, Y. Chen, *J. Am. Ceram. Soc.* **2021**, *104*, 5537.
[10] a) J. K. El-Demellawi, S. Lopatin, J. Yin, O. F. Mohammed, H. N. Alshareef, *ACS Nano* **2018**, *12*, 8485; b) V. Mauchamp, M. Bugnet, E. P. Bellido, G. A. Botton, P. Moreau, D. Magne, M. Naguib, T. Cabioc'h, M. W. Barsoum, *Phys. Rev. B* **2014**, *89*, 235428; c) Y. Dong, S. Chertopalov, K. Maleski, B. Anasori, L. Hu, S. Bhattacharya, A. M. Rao, Y. Gogotsi, V. N. Mochalin, R. Podila, *Adv. Mater.* **2018**, *30*, 1705714.
[11] C. Wu, A. B. Khanikaev, R. Adato, N. Arju, A. A. Yanik, H. Altug, G. Shvets, *Nat. Mater.* **2011**, *11*, 69.
[12] a) X. Yang, Z. Sun, T. Low, H. Hu, X. Guo, F. J. Garcia de Abajo, P. Avouris, Q. Dai, *Adv. Mater.* **2018**, *30*, e1704896; b) D. Rodrigo, O. Limaj, D. Janner, D. Etezadi, F. J. García De Abajo, V. Pruneri, H. J. S. Altug, *Science* **2015**, *349*, 165.
[13] a) J. Yi, J. Li, S. Huang, L. Hu, L. Miao, C. Zhao, S. Wen, V. N. Mochalin, A. M. Rao, *InfoMat* **2019**, *2*, 601; b) Q. Wu, S. Chen, Y. Wang, L. Wu, X. Jiang, F. Zhang, X. Jin, Q. Jiang, Z. Zheng, J. Li, M. Zhang, H. Zhang, *Adv. Mater. Technol.* **2019**, *4*, 1800532; c) X. Jiang, S. Liu, W. Liang, S. Luo, Z. He, Y. Ge, H. Wang, R. Cao, F. Zhang, Q. Wen, J. Li, Q. Bao, D. Fan, H. Zhang, *Laser Photonics Rev.* **2017**, *12*, 1700229; d) B. Fu, J. Sun, C. Wang, C. Shang, L. Xu, J. Li, H. Zhang, *Small* **2021**, *17*, e2006054.
[14] N. Li, X. Guo, X. Yang, R. Qi, T. Qiao, Y. Li, R. Shi, Y. Li, K. Liu, Z. Xu, L. Liu, F. J. García de Abajo, Q. Dai, E. G. Wang, P. Gao, *Nat. Mater.* **2021**, *20*, 43.
[15] X. Guo, H. Hu, D. Hu, B. Liao, K. Chen, L. Liu, X. Zhu, X. Yang, Q. Dai, *Nanoscale* **2019**, *11*, 2703.
[16] S. Dai, Z. Fei, Q. Ma, A. S. Rodin, M. Wagner, A. S. McLeod, M. K. Liu, W. Gannett, W. Regan, K. Watanabe, T. Taniguchi, M. Thiemens, G. Dominguez, A. H. Castro Neto, A. Zettl, F. Keilmann, P. Jarillo-Herrero, M. M. Fogler, D. N. Basov, *Science* **2014**, *343*, 1125.
[17] L. Liang, W. Gu, Y. Wu, B. Zhang, G. Wang, Y. Yang, G. Ji, *Adv. Mater.* **2022**, *34*, 2106195.
[18] R. Qi, R. Wang, Y. Li, Y. Sun, S. Chen, B. Han, N. Li, Q. Zhang, X. Liu, D. Yu, P. Gao, *Nano Lett.* **2019**, *19*, 5070.
[19] X. Yang, F. Zhai, H. Hu, D. Hu, R. Liu, S. Zhang, M. Sun, Z. Sun, J. Chen, Q. Dai, *Adv. Mater.* **2016**, *28*, 2931.
[20] H. Yan, T. Low, W. Zhu, Y. Wu, M. Freitag, X. Li, F. Guinea, P. Avouris, F. Xia, *Nature Photon.* **2013**, *7*, 394.
[21] J. Luo, W. Zhang, H. Yuan, C. Jin, L. Zhang, H. Huang, C. Liang, Y. Xia, J. Zhang, Y. Gan, X. Tao, *ACS Nano* **2017**, *11*, 2459.
[22] G. Yang, D. Liu, C. Chen, Y. Qian, Y. Su, S. Qin, L. Zhang, X. Wang, L. Sun, W. Lei, *ACS Nano* **2021**, *15*, 6594.
[23] Y. Ma, N. Liu, L. Li, X. Hu, Z. Zou, J. Wang, S. Luo, Y. Gao, *Nat. Commun.* **2017**, *8*, 1207.
[24] S. Huang, R. Shi, Y. Li, M. Wu, N. Li, J. Du, D. Yu, P. Gao, *Chin. J. Vac. Sci. Technol.* **2021**, *41*, 213.
[25] W. Dong, R. Qi, T. Liu, Y. Li, N. Li, Z. Hua, Z. Gao, S. Zhang, K. Liu, J. Guo, P. Gao, *Adv. Mater.* **2020**, *32*, 2002014.
[26] A. A. Govyadinov, A. Konecna, A. Chuvilin, S. Velez, I. Dolado, A. Y. Nikitin, S. Lopatin, F. Casanova, L. E. Hueso, J. Aizpurua, R. Hillenbrand, *Nat. Commun.* **2017**, *8*, 95.
[27] F. J. García de Abajo, *Rev. Mod. Phys.* **2010**, *82*, 209.